Shape Optimization of Adhesives of Multi-materials under Multiaxial Stress Failure Criteria

Yang Xue[a], Hiro Tanaka[a],

Yoji Shibutani[a,b]

[a]*Department of Mechanical Engineering, Osaka University, Japan*;

[b]*Nanotechnology Program, Vietnam Japan University, VNU*

Address correspondence to Yoji Shibutani, Department of Mechanical Engineering, Osaka University, 2-1, Yamadaoka, Suita, Osaka, 565-0871, Japan. E-mail: sibutani@mech.eng.osaka-u.ac.jp

Shape Optimization of Adhesives of Multi-materials under Multiaxial Stress Failure Criteria

In recent years, multi-material design concept has been applied to many industries. Among various methods of joining dissimilar materials, adhesive bonding is quite suitable for the purpose of lightening the weight. In order to choose the most preferable adhesive for improvement of the strength, it is necessary to understand the failure criteria of adhesives. Experiments using pipe specimens with inclined surfaces bonded by an epoxy adhesive were performed, which can achieve multiaxial stress states while solely recurring to a uniaxial tensile test. The failure function of the epoxy adhesive, expressed by the mean stress and octahedral shear stress, was then obtained from the experiment data and compared with that of the acrylic adhesive in the previous research. The failure functions of both adhesives were then applied to the shape optimization of the adhesive layer under different loading conditions. The optimization object is to improve the strength of bonded structures. The optimal shape for different loading conditions differs for each adhesive because of the driving force due to the applied stress. Thus, the final shapes are numerically optimized to attain the highest mechanical integrity of the adhesive layer and show strong dependences on the initial shapes prior to optimization.

Keywords: Adhesive; Epoxy adhesive; Acrylic adhesive; Failure criterion; Multiaxial stress state; Shape optimization

Introduction

In recent years, one of the most important technical trends of the automotive industry is to reduce the weight of structures so that emission of carbon-dioxide and energy consumption are also reduced. One strategy to lighten the structures is multi-material design [1], that is, the combination of different materials with appropriate strength and stiffness. Multi-material design is generally applied to the flame of structures where the strength of the bonded parts is crucial. In order to join dissimilar materials, several methods have been developed such as laser welding [2], friction stir

spot welding [3], and combination of mechanical fastening with bolts and adhesive bonding [4]. Adhesive bonding is one of the most promising joining methods, which is widely used to bond materials with dissimilar properties together because the adhesive materials are lighter than other mechanical fastenings. There are many kinds of adhesives while two major groups are most widely used in many industries, epoxy and acrylic adhesives. The former is a typical and major one of structural adhesives, which can provide a high-performance for bonding large areas of sheet materials and produce a better finished appearance than the other joint methods such as welding or screws [5]. Epoxy adhesives are widely used in various industries especially for large size products such as aerospace, automotive and marine where higher strength is required. Acrylic adhesive used in the construction sector is an adhesive bond that comprises a denatured acrylic-based structural adhesive of 2-component type. As the molecular structures of these two adhesives are different, so too are their physical and mechanical properties. [6, 7]

In order to understand the mechanical properties of epoxy and acrylic adhesives, adhesive failure assessment based on multiaxial stress states should be considered in the practical multiple material design. Therefore, the conventional lap joint tests are not accurate to perform structural design. Some failure criteria have been proposed such as quadratic stress criterion [8] and other stress-based failure criteria [9-12]. However, they have unknown parameters which are dependent on the properties of adhesive materials. As a result, it is necessary to identify those parameters from experiments before further research of adhesives. Those for the acrylic adhesive have been experimentally determined using pipe specimens which can tune the ratio of applied mean stress and shear stress to realize multiaxial stress state in the previous research. [13]. Also, the strength of adhesives is highly influenced by its thickness, the parent materials adhered

as well as the material property of adhesives. These complex factors suggest that mechanical integrity of bonded structures should be required. Therefore, a shape optimization of the adhesive interface was proposed to improve the strength of bonded structure under the proposed failure criterion. Some shape optimizations of adhesive layer have been demonstrated according to the failure criterion of acrylic adhesive. [14]

As the strength of adhesives is influenced by both material and structural factors, this research aims to involve both these two factors and to discuss how those factors affect the strength of bonded structures. an epoxy adhesive is investigated using the same as the previous research [13], and the parameters defined in the failure criteria are experimentally determined. The comparison of adhesive materials between epoxy and acrylic adhesives was performed to identify the difference in the failure behaviors in multiaxial stress states. The shape optimization using the failure criteria obtained from the experimental data was also performed to improve the strength of structure, reflecting the difference of each adhesive's properties.

Failure Criterion of Adhesive

In order to measure the strength of the adhesive layer, tests have been executed using lap joint tests such as single-lap shear test [15-17] and peel test [18,19]. However, these tests regard stress distribution in the finite adhesive layer which allows a stress singularity occurring at the free edge. As a result, these measurements are not appropriate to fit the failure criterion. To avoid the stress concentration effect, a shear stress test using a napkin-ring specimen has been proposed [20-23] and used in a tension-torque test method [24, 25] so that the failure criterion in multiaxial stress state can be estimated by experimental results. It is a good way to evaluate the failure criterion without a free-edge effect, but this method requires a highly accurate biaxial

testing machine which may be difficult to access for most institutions generally. In order to realize a multiaxial stress state only by using a simple uniaxial tensile test, a new method using cylindrical pipe specimens with inclined cutting surface has been developed [13].

In the present paper, two cylindrical coordinate systems are established with two kinds of loadings, uniaxial tension and torque, but only the former is applied for the experiments to get the failure function and the obtained criteria are extended to the shape optimization of adhesives under the two kinds of loadings. The cylindrical coordinate system (r, θ, z) are transformed into (r', θ', z') in terms of the angle φ between the horizontal plane $r\theta$ and the inclined plane $r'\theta'$ parallel to the adhesive surface as shown in Fig. 1.

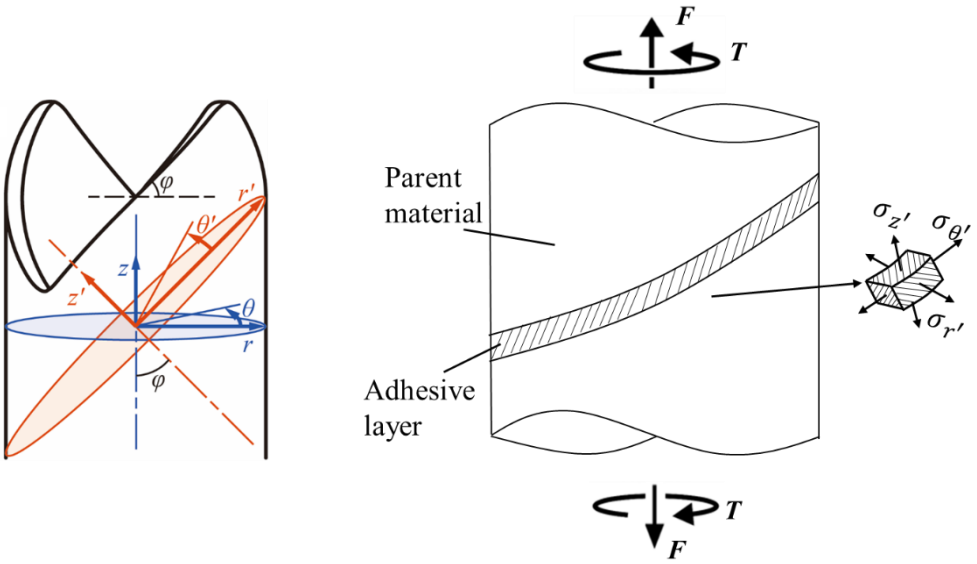

Figure 1. Coordinate transformation of the cylindrical coordinate system from (r, θ, z) to (r', θ', z') in terms of angle φ. [13]

Because the thickness of adhesive layer is small enough and the stiffness of adhesive is much smaller than that of the parent material, the deformation of adhesive is assumed to be strongly restricted by the more rigid parent material. Then, the normal

strains acting in the radial and circumferential directions along the cutting surface can be assumed that:

$$\frac{\varepsilon_{r'}}{\varepsilon'_z} \approx 0, \tag{1}$$

$$\frac{\varepsilon_{\theta'}}{\varepsilon'_z} \approx 0. \tag{2}$$

This assumption has been certified using finite element simulations for Poisson's ratio with a range from 0.2 to 0.4 [13]. Constitutive equations are then derived from Eqs. (1) and (2):

$$\sigma_{r'} = \sigma_{\theta'} = \frac{E\nu}{(1+\nu)(1-2\nu)}\varepsilon_{z'}, \qquad \sigma_{z'} = \frac{E(1-\nu)}{(1+\nu)(1-2\nu)}\varepsilon_{z'}. \tag{3}$$

where $\sigma_{r'}$, $\sigma_{\theta'}$ and $\sigma_{z'}$ are the normal stresses in radial, circumferential and direction along the cutting surface, and E is Young's modulus and ν is Poisson's ratio. According to Eq. (3), $\sigma_{r'}$ and $\sigma_{\theta'}$ are expressed as a function of $\sigma_{z'}$.

$$\sigma_{r'} = \sigma_{\theta'} = \frac{\nu}{1-\nu}\sigma_{z'}. \tag{4}$$

The first invariant of stress tensor I_1 and the second invariant of deviatoric stress tensor J_2 can be calculated as:

$$I_1 = \sigma_{r'} + \sigma_{\theta'} + \sigma_{z'} = \frac{1+\nu}{1-\nu}\sigma_{z'}, \tag{5}$$

$$\begin{aligned} J_2 &= \frac{1}{2}\left\{\left(\sigma_{r'}^2 + \sigma_{\theta'}^2 + \sigma_{z'}^2 + 2\tau_{r'\theta'}^2 + 2\tau_{\theta'z'}^2 + 2\tau_{z'r'}^2\right) - \frac{1}{3}I_1^2\right\} \\ &= \frac{1}{3}\left(\frac{1-2\nu}{1-\nu}\right)^2 \sigma_{z'}^2 + \tau_{\theta'z'}^2. \end{aligned} \tag{6}$$

Here, in Eq. (6), $\tau_{r'\theta'}$ and $\tau_{z'r'}$ are assumed to be infinitesimally small compared with $\tau_{\theta'z'}$ and $\sigma_{z'}$.

According to the coordinate transformation in Fig.1, the normal stress $\sigma_{z'}$ and shear stress $\tau_{\theta' z'}$ acting in the adhesive layer can be expressed by the tensor transformation as:

$$\sigma_{z'} = \frac{\sigma_z}{2} + \frac{\sigma_z}{2}\cos 2\varphi - \tau \sin 2\varphi\,, \tag{7}$$

$$\tau_{\theta' z'} = -\frac{\sigma_z}{2}\sin 2\varphi - \tau \cos 2\varphi\,. \tag{8}$$

For a uniaxial tensile test mentioned in the following chapter, only the tensile stress σ_z exists. Thus, according to Eqs. (7) and (8), $\sigma_{z'}$ and $\tau_{\theta' z'}$ can be calculated as:

$$\sigma_{z'} = \sigma_z \cos^2 \varphi\,, \tag{9}$$

$$\tau_{\theta' z'} = \sigma_z \sin \varphi \cos \varphi\,. \tag{10}$$

From Eqs. (5) and (6), I_1 and J_2 are reduced to be the following linear relation:

$$\sqrt{J_2} = \left\{ \frac{1-\nu}{1+\nu} \sqrt{\frac{1}{3}\left(\frac{1-2\nu}{1-\nu}\right)^2 + \tan^2 \varphi} \right\} I_1 = k(\varphi, \nu) I_1, \tag{11}$$

where $k(\varphi, \nu)$ is the coefficient which can be calculated from angle φ and Poisson's ratio ν. In the following results, mean stress $\sigma_m \left(= \frac{1}{3} I_1\right)$ and octahedral shear stress $\tau_{\mathrm{oct}} \left(= \sqrt{\frac{2}{3} J_2}\right)$ are employed instead of I_1 and J_2 for the practical usage.

The failure function proposed by Mahnken and Schlimmer [9, 13] is

$$f = C_0 J_2 + \frac{1}{3} C_1 I_1 + \frac{1}{3} C_2 {I_1}^2 + C_3. \tag{12}$$

If the parameters are taken as $C_1 = 0$ and $C_2 \neq 0$, the obtained failure criterion is the same as the one proposed by Green [26] which can be considered as equivalent to the quadratic delamination criterion proposed by Brewer and Lagace [27]. If $C_1 = C_2 = 0$, the failure function is equivalent to the conventional von Mises failure criteria.

From Eqs. (5) and (6), it is clearly shown that the failure function can be estimated with three parameters of v, φ and σ_z, which are determined by the results of tensile tests using the pipe specimens bonded by different adhesives. Poisson's ratios v of the adhesives are taken into the present research as 0.35 for epoxy adhesive and 0.4 for acrylic adhesive, respectively. As the failure criterion differs only by the parameters, the numbers of 1/3 before the coefficients of C_1 and C_2 in Eq. (12) do not have any meaning. As a result, the failure criterion can be simplified as:

$$f = c_0 J_2 + c_1 I_1 + c_2 {I_1}^2 + c_3. \tag{13}$$

where $c_0 = C_0$, $c_1 = \frac{1}{3} C_1$, $c_2 = \frac{1}{3} C_2$ and $c_3 = C_3$.

Shape Optimization

In order to perform the shape optimal design of adhesive structures which is induced to minimize the stress operated in the adhesive layer under the multiaxial stress state, the objective function should be formulated [14]. The multi-material region with the adhesive layer is shown in Fig. 2.

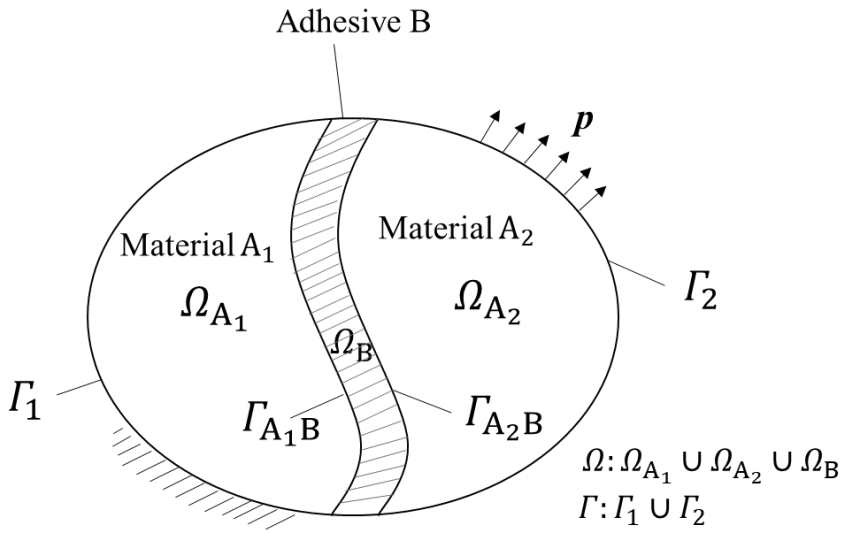

Figure 2. Multi-material model consisting of two materials of A_1 and A_2 bonded by adhesion of *B*; suppose that traction *p* is applied at boundary Γ_2 and body force *f* acts in Ω. The region is kinematically supported at boundary Γ_1.

The following governing equations including equilibrium equation, boundary conditions and continuity conditions at the interface hold in the region $\Omega_m (m = \mathrm{A}_1, \mathrm{A}_2, \mathrm{B})$ with the boundary region of Γ_1, Γ_2 and $\Gamma_{m\mathrm{B}}$ $(m = \mathrm{A}_1, \mathrm{A}_2)$ in Fig. 2.

$$\sigma_{ij,j}^m + f_i = 0 \text{ in } \Omega_m \ (m = \mathrm{A}_1, \mathrm{A}_2, \mathrm{B}), \tag{14}$$

$$u_i = 0 \text{ on } \Gamma_1, \tag{15}$$

$$\sigma_{ij} n_j = p_i \text{ on } \Gamma_2, \tag{16}$$

$$\sigma_{ij}^m n_j^m = -\sigma_{ij}^B n_j^B \text{ on } \Gamma_{m\mathrm{B}} \ (m = \mathrm{A}_1, \mathrm{A}_2). \tag{17}$$

Here, $\boldsymbol{p}$ is the surface traction vector, $\boldsymbol{f}$ is the body force vector and $\boldsymbol{n}$ is the normal vector of the boundary. The linear and bilinear functions are defined as following:

$$a_m(\boldsymbol{u}, \boldsymbol{v}) = \int_{\Omega_m} \sigma_{ij}^m(\boldsymbol{u}) \varepsilon_{ij}^m(\boldsymbol{v}) d\Omega \ (m = \mathrm{A}_1, \mathrm{A}_2, \mathrm{B}), \tag{18}$$

$$l(\boldsymbol{v}) = \int_{\Gamma_2} p_i v_i d\Gamma + \int_{\Omega} f_i v_i \, d\Omega, \tag{19}$$

$$h_{1m}(\boldsymbol{u}, \boldsymbol{v}) = \int_{\Gamma_{A_1 B}} \sigma_{ij}^m(\boldsymbol{u}) n_j^m v_i d\Gamma \ \ (m = \mathrm{A}_1, \mathrm{B}), \tag{20}$$

$$h_{2m}(\boldsymbol{u}, \boldsymbol{v}) = \int_{\Gamma_{A_2 B}} \sigma_{ij}^m(\boldsymbol{u}) n_j^m v_i d\Gamma \ \ (m = \mathrm{A}_2, \mathrm{B}), \tag{21}$$

where $\boldsymbol{v}$ is an adjoint variable of the function space $\boldsymbol{\mathcal{U}}$ expressed by the following equation:

$$\boldsymbol{\mathcal{U}} = \{\boldsymbol{v} \in H^1(\Omega;\, \mathcal{R}^3) | \boldsymbol{v} = 0 \text{ on } \Gamma_1\}. \tag{22}$$

The governing Eqs. (14) to (16) can be expressed using Eqs. (18) to (21) based on the principal of virtual work.

$$\begin{gathered} a_{A_1}(\boldsymbol{u},\boldsymbol{v}) - h_{1\mathrm{A}_1}(\boldsymbol{u},\boldsymbol{v}) + a_{\mathrm{A}_2}(\boldsymbol{u},\boldsymbol{v}) - h_{2\mathrm{A}_2}(\boldsymbol{u},\boldsymbol{v}) + \\ a_B(\boldsymbol{u},\boldsymbol{v}) - h_{1\mathrm{B}}(\boldsymbol{u},\boldsymbol{v}) - h_{2\mathrm{B}}(\boldsymbol{u},\boldsymbol{v}) - l(\boldsymbol{v}) = 0, \forall \boldsymbol{v} \in \boldsymbol{\mathcal{U}}. \end{gathered} \tag{23}$$

The displacement $\boldsymbol{u}$ required to calculate the objective function must always satisfy the above governing Eq. (23).

It is assumed that $\boldsymbol{v}$ is a continuous function on the interface $\Gamma_{\mathrm{A}_1\mathrm{B}}$ and $\Gamma_{\mathrm{A}_2\mathrm{B}}$ as follows:

$$v^m = v^B \text{ on } \Gamma_{m\mathrm{B}}\ (m = \mathrm{A}_1, \mathrm{A}_2). \tag{24}$$

Then, according to Eqs. (17) and (24), governing Eq. (23) can be simplified as:

$$a_{\mathrm{A}_1}(\boldsymbol{u},\boldsymbol{v}) + a_{\mathrm{A}_2}(\boldsymbol{u},\boldsymbol{v}) + a_{\mathrm{B}}(\boldsymbol{u},\boldsymbol{v}) - l(\boldsymbol{v}) = 0, \forall \boldsymbol{v} \in \boldsymbol{\mathcal{U}}. \tag{25}$$

The failure function f based on Eq. (13) has a different value dependent to the stresses occurring in the adhesive layer and the failure happens when $f = 0$. In order to enhance the strength of the adhesive structure, the values of failure function f are supposed to become uniform throughout the adhesive layer for the applied stress to be minimized as much as possible. Therefore, the object function is to minimize it in the adhesive layer region Ω_B as the sum of squares of failure function f occurring in the whole adhesive layer as follows [14].

$$\text{Find } \Omega_{\mathrm{B}} : \min_{\Omega_{\mathrm{B}}} F \text{, where } F = \frac{\int_{\Omega_{\mathrm{B}}} (f - c_3)^2 d\Omega}{\int_{\Omega_{\mathrm{B}}} d\Omega}. \tag{26}$$

In order to avoid diminishment and disappearance of the adhesive layer region Ω_B, the constant volume constraint on Ω_B is imposed. As a result, the shape optimization problem of the adhesive interface for the multi-material region becomes the following formulas.

$$\min_{\Omega_{\mathrm{B}}} F(I_1, J_2),$$

$$\text{subject to Boundary} - \text{value problem and} \tag{27}$$

$$V_{\mathrm{B}} = \bar{V}_{\mathrm{B}} \text{ where } V_{\mathrm{B}} = \int_{\Omega_{\mathrm{B}}} d\Omega.$$

where $\bar{V}_B$ is the initial volume of the adhesive layer.

The traction method [28] is used to calculate the adjoint velocity field $\boldsymbol{\mathcal{V}}$. For this purpose, it is necessary to derive the shape gradient function that acts as an external force term in the traction method. According to the optimization problem set in Eq. (27), a Lagrange functional is defined as:

$$L = \frac{\int_{\Omega_{\mathrm{B}}} (f - c_3)^2 d\Omega}{\int_{\Omega_{\mathrm{B}}} d\Omega} - \left[\begin{matrix} a_{\mathrm{A}_1}(\boldsymbol{u}, \boldsymbol{v}) - h_{1\mathrm{A}_1}(\boldsymbol{u}, \boldsymbol{v}) + a_{\mathrm{A}_2}(\boldsymbol{u}, \boldsymbol{v}) - h_{2\mathrm{A}_2}(\boldsymbol{u}, \boldsymbol{v}) \\ + a_B(\boldsymbol{u}, \boldsymbol{v}) - h_{1\mathrm{B}}(\boldsymbol{u}, \boldsymbol{v}) - h_{2\mathrm{B}}(\boldsymbol{u}, \boldsymbol{v}) - l(\boldsymbol{v}) \end{matrix} \right]$$
$$+ \Lambda(V_{\mathrm{B}} - \bar{V}_{\mathrm{B}}). \tag{28}$$

Here, Λ is the undetermined multiplier of Lagrange. Then, the time derivative of the Lagrange functional $\dot{L}$ for the domain variation according to the velocity field $\boldsymbol{\mathcal{V}}$ becomes the following formula:

$$\dot{L} = -[a_{\mathrm{A}_1}(\boldsymbol{u}, \boldsymbol{v}') + a_{\mathrm{A}_2}(\boldsymbol{u}, \boldsymbol{v}') + a_{\mathrm{B}}(\boldsymbol{u}, \boldsymbol{v}') - l(\boldsymbol{v}')]$$

$$- \left[a_{\mathrm{A}_1}(\boldsymbol{u}', \boldsymbol{v}) + a_{\mathrm{A}_2}(\boldsymbol{u}', \boldsymbol{v}) + a_{\mathrm{B}}(\boldsymbol{u}', \boldsymbol{v}) - \frac{2\int_{\Omega_{\mathrm{B}}} f'(f - c_3)^2 d\Omega}{\int_{\Omega_{\mathrm{B}}} d\Omega} \right]$$
$$+ \Lambda'(V_{\mathrm{B}} - \bar{V}_{\mathrm{B}}) + l_G(\boldsymbol{\mathcal{V}}), \tag{29}$$

$$l_G(\boldsymbol{\mathcal{V}}) = \int_{\Gamma_{\mathrm{A_1B}}} G_{\mathrm{A_1B}}\, \boldsymbol{n}\cdot\boldsymbol{\mathcal{V}}\mathrm{d}\Gamma + \int_{\Gamma_{\mathrm{A_2B}}} G_{\mathrm{A_2B}}\, \boldsymbol{n}\cdot\boldsymbol{\mathcal{V}}\mathrm{d}\Gamma, \tag{30}$$

$$G_{m\mathrm{B}} = \frac{(f-c_3)^2}{\int_{\Omega_\mathrm{B}} d\Omega} - \frac{\int_{\Omega_\mathrm{B}}(f-c_3)^2 d\Omega}{\left(\int_{\Omega_\mathrm{B}} d\Omega\right)^2} - \left[\sigma_{ij}^{\mathrm{B}}(\boldsymbol{u})\varepsilon_{ij}^{\mathrm{B}}(\boldsymbol{v}) - \sigma_{ij}^{m}(\boldsymbol{u})\varepsilon_{ij}^{m}(\boldsymbol{v})\right] + \sigma_{ij}^{\mathrm{B}} n_j^{\mathrm{B}}\left(v_{i,k}^{\mathrm{B}} - v_{i,k}^{m}\right) n_k^{\mathrm{B}} + \Lambda \ (m = \mathrm{A_1}, \mathrm{A_2}), \tag{31}$$

where it recalls that $(\cdot)'$ denotes the partial derivative for region variation. From Eq. (29), the term of the velocity field $\boldsymbol{\mathcal{V}}$ can be expressed by the shape gradient function $G_{\mathrm{A_1B}}$ and $G_{\mathrm{A_1B}}$ on the adhesive interface $\Gamma_{\mathrm{A_1B}}$ and $\Gamma_{\mathrm{A_2B}}$. According to Eq. (29), the optimal condition for $\boldsymbol{u}$, $\boldsymbol{v}$ and Λ of the Lagrange functional L is

$$a_{\mathrm{A_1}}(\boldsymbol{u}, \boldsymbol{v}') + a_{\mathrm{A_2}}(\boldsymbol{u}, \boldsymbol{v}') + a_{\mathrm{B}}(\boldsymbol{u}, \boldsymbol{v}') - l(\boldsymbol{v}') = 0, \forall \boldsymbol{v}' \in \boldsymbol{\mathcal{U}}, \tag{32}$$

$$a_{\mathrm{A_1}}(\boldsymbol{u}', \boldsymbol{v}) + a_{\mathrm{A_2}}(\boldsymbol{u}', \boldsymbol{v}) + a_{\mathrm{B}}(\boldsymbol{u}', \boldsymbol{v}) - \frac{2\int_{\Omega_B} f'(f-c_3)^2 d\Omega}{\int_{\Omega_\mathrm{B}} d\Omega} = 0, \forall \boldsymbol{u}' \in \boldsymbol{\mathcal{U}}, \tag{33}$$

$$\Lambda'(V_\mathrm{B} - \bar{V}_\mathrm{B}) = 0. \tag{34}$$

Here Eq. (32) has the same meaning with the governing equation (25) calculating the displacement $\boldsymbol{u}$ by FEM analysis. Eq. (33) is the adjoint equation of the adjoint variable vector $\boldsymbol{v}$ and Eq. (34) is the constraint condition of the volume. According to the symmetry of a_m $(m = \mathrm{A_1}, \mathrm{A_2})$ and the chain rule of partial derivative, Eq. (33) can be written as:

$$a_{\mathrm{A_1}}(\boldsymbol{v}, \boldsymbol{u}') + a_{\mathrm{A_2}}(\boldsymbol{v}, \boldsymbol{u}') + a_{\mathrm{B}}(\boldsymbol{v}, \boldsymbol{u}') - l_2(\boldsymbol{u}') = 0, \tag{35}$$

where $l_2(\boldsymbol{u}') = \int_{\Omega_B} \frac{2\int_{\Omega_\mathrm{B}} f'(f-c_3)^2 d\Omega}{\int_{\Omega_\mathrm{B}} d\Omega} \frac{\partial f}{\partial \sigma_{ij}} \frac{\partial \sigma_{ij}}{\partial \boldsymbol{u}_k} \boldsymbol{u}'_k d\Omega, \forall \boldsymbol{u}' \in \boldsymbol{\mathcal{U}}$.

According to Eq. (35), the term of the external force l is replaced by l_2 and the adjoint variable vector $\boldsymbol{v}$ can be calculated by FEM analysis.

Finally, the velocity field $\boldsymbol{\mathcal{V}}$ is calculated, which is used to update the shape of the adhesive layer according to the traction method as

$$a(\boldsymbol{\mathcal{V}}, \boldsymbol{w}) = -l_G(w), \boldsymbol{\mathcal{V}} \in C_{\boldsymbol{\Theta}}, \forall \boldsymbol{w} \in C_{\boldsymbol{\Theta}}. \quad (36)$$

Here, $a(\boldsymbol{\mathcal{V}}, \boldsymbol{w})$ is the property value of adhesives, $l_G(\boldsymbol{w})$ is obtained according to Eq. (30) and $C_{\boldsymbol{\Theta}}$ is the allowable function space that satisfies the constraint condition of region variation.

The flowchart of the numerical analysis for optimization is shown in Fig. 3 [14]. The displacement field $\boldsymbol{u}$ satisfying Eq. (32) is calculated by FEM analysis. The values of stress calculated from the FEM analysis are input into the failure function f of Eq. (13) and the objective function F is calculated. The result is then compared with the value of F in the previous step. If the difference of the values between the two steps is larger than 10^{-3}, the analysis keeps going. The vector field $\boldsymbol{v}$ which satisfies the adjoint equation (35) is calculated by FEM analysis. The obtained displacement field $\boldsymbol{u}$ and vector field $\boldsymbol{v}$ are used to calculate the shape gradient function according to Eq. (31). The velocity field $\boldsymbol{\mathcal{V}}$ is then obtained from Eq. (36) by the traction method and is used to update the shape of the interface. The iteration keeps going until the change rate of objective function is less than 10^{-3}. Finally, the output result is the optimal design of the adhesive interface.

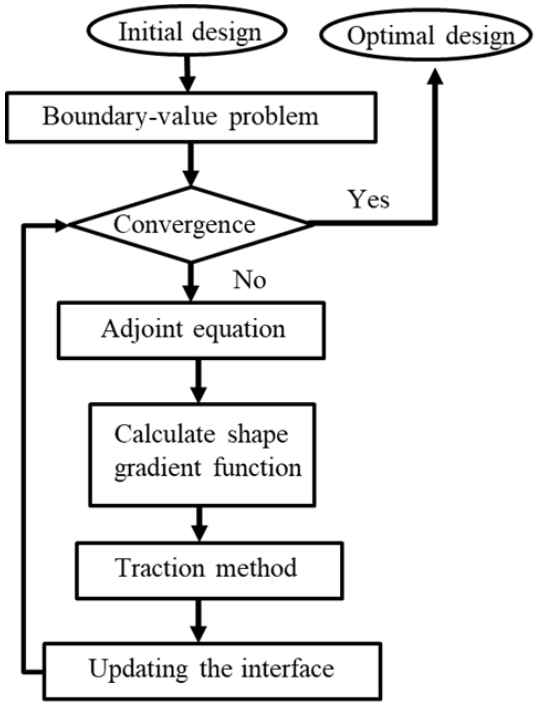

Figure 3. The flowchart of the shape optimization process. The iteration will keep going on until the change rate of F is less than 10^{-3}.

Failure Criterion Obtained from Experiments

Experiment using pipe specimens

The parameters of the failure criterion of Eq. (13) for acrylic adhesive (HardlocTM: M-600-08, Denka Co., Ltd.) were already determined by the experiments in ref. [13]. The same experiments are performed using pipe specimens with inclined cutting surfaces bonded by epoxy adhesive (EP-171, CEMEDINE Co., Ltd.), which can realize the multiaxial stress states only by a uniaxial tensile test. A5052 aluminum pipe specimens, which have the tilted cutting surfaces by laser processing with the inclination angles φ of 20°, 45° and 75°, are shown in Fig. 4 (a). The outer radius and thickness of the pipe specimens are 45 mm and 3 mm, respectively. The load-displacement curves obtained from the tensile tests (see Fig. 4 (b)) with the strain rate of

5.56×10^{-3} [/s] are also shown in Fig. 5. The response of epoxy adhesive is almost linear compared with the case of acrylic adhesive with nonlinear response and shows the very sharp maximum point regardless of the thickness *h* of adhesive layer. In general, the fracture of adhesive layer has the visco-plastic characterization with mean pressure dependence because the void nucleation and its growth behaviors might be essential. As a result, the proportional limit as the rather clear threshold between the linear elastic and the nonlinear parts is adopted in this research.

(a) Test specimens

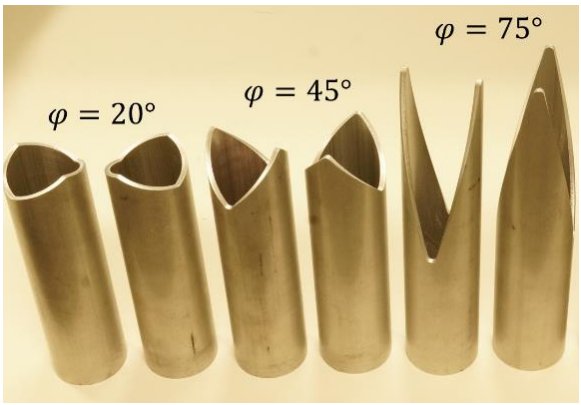

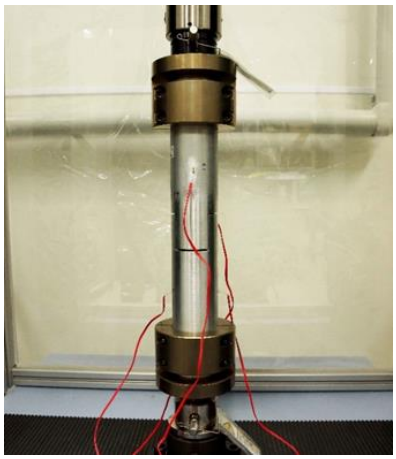

(b) Tensile test process

Figure 4. (a) Test specimens with inclined cutting surfaces and (b) tensile test process.

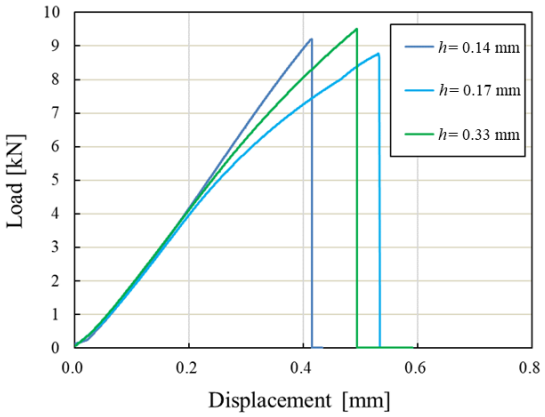

(a)

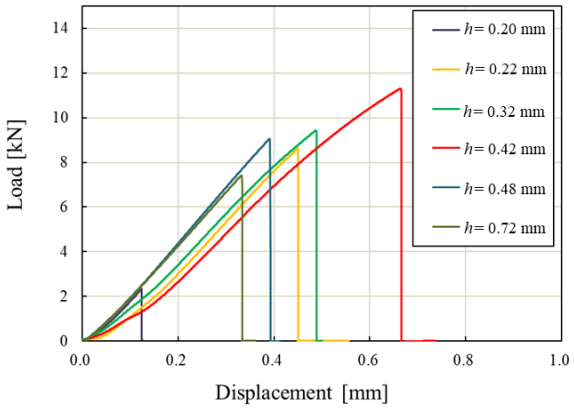

(b)

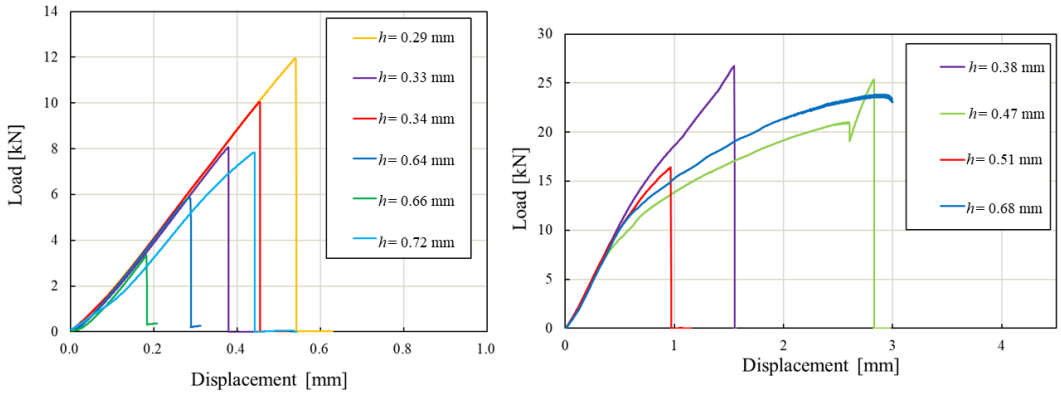

(c) (d)

Figure 5. Load-displacement curves obtained from experiments; (a) $\varphi = 0°$, (b) $\varphi = 20°$, (c) $\varphi = 45°$, (d) $\varphi = 75°$.

Failure criterion

I_1 and J_2 are calculated by the results of experiments according to Eqs. (5), (6), (7) and (8). The parameters c_1, c_2, and c_3 are estimated by the least squares fit as it is a quadratic function. According to the fitting, the parameters for the epoxy adhesive are newly obtained; c_1 is -9.03 [MPa], c_2 is 0.199 and c_3 is -11.5 [MPa^2] under c_0=1.00. The failure curve is obtained by $f = 0$, as shown in Fig. 6 (a) with Poisson's ratio v of 0.35 and the reference thickness because each sample has a different thickness in the manufacturing process. The previous result for acrylic adhesive with v = 0.4 is drawn in Fig. 6 (b) as a reference with $c_1 = -0.200$ [MPa], $c_2 = 0.0590$ and $c_3 = -14.0$ [MPa^2] under $c_0 = 1.00$. The failure criteria were established only from the experimental data collected from single-material pipes. In present research, the failure function is also established from multi-material pipe specimens and compared with the previous results to check if the failure function established from single-material pipes is also applicable. Fig. 6 is denoted using σ_m and τ_{oct} instead of I_1 and J_2 due to easier understanding of their magnitudes. The relationships between both quantities are

expressed as $\sigma_m = \frac{1}{3} I_1$ and $\tau_{\mathrm{oct}} = \sqrt{\frac{2}{3} J_2}$. Comparing these two curves, it is obvious that there is a relative maximum point at the case of epoxy adhesive, which shows the largest value τ_{oct} at some nonzero value of σ_m. As a result, the failure function can be rewritten as:

$$f = c_0' \tau_{\mathrm{oct}}^2 + c_2' (\sigma_m - c_1')^{\,2} + c_3', \tag{37}$$

Where $c_0' = \frac{3}{2} c_0$, $c_1' = -\frac{c_1}{6c_2}$, $c_2' = 9c_2$ and $c_3' = c_3 - \frac{c_1^2}{4c_2}$. The new parameters are $c_1' = 7.56$ [MPa], $c_2' = 1.79$ and $c_3' = -114$ [MPa^2] under $c_0' = 1.5$ for the epoxy, while on the other hand, $c_1' = 0.56$ [MPa], $c_2' = 0.531$ and $c_3' = -14.2$ [MPa^2] under $c_0' = 1.5$ for the acrylic using the data obtained in ref. [13]. c_1' suggests how large the hydrostatic pressure (mean stress) affects the maximum distorsional strength of adhesive material. The former is much larger than the latter and thus the epoxy adhesive can provide the maximum strength under dilatation circumstance of around 7.6 [MPa]. Recall that some linear dashed lines in Fig. 6 show the relationship of Eq. (11). Each slope equals to $\sqrt{6}k$, where $k(\varphi, v)$ is in Eq. (11) and determined only by the different angle φ for the same Poisson's ratio.

Whenever the failure of materials is discussed, it is usually determined only by the intrinsic strength of materials such as yield stress. However, in the adhesive problem, the factors affecting the strength are not only properties of adhesive materials but also the other geometric factors of structure. Among those factors, thickness of adhesive layer has the most significant effect. As a result, the failure function should be reconsidered as it is not applicable to adhesive layers with different thickness [29]. A scale function, δ, which extends the failure criterion of Eq. (13) to different adhesive layer thickness, has been formulated based on the reference thickness h^*[30]:

$$\delta = \frac{(\sigma_m - x_0)^2}{a^2} + \frac{{\tau_{\mathrm{oct}}}^2}{b^2},$$

$$\text{where } |a| = \frac{1}{3}\sqrt{\frac{c_1^2}{4c_2^2} - \frac{c_3}{c_2}}, |b| = \sqrt{\frac{c_1^2}{36c_2^2} - c_3} \text{ and } x_0 = -\frac{c_1}{6c_2}. \quad (38)$$

δ was set to 1 when a point (σ_m, τ_{oct}) is located on the curve of failure function. All the failure magnitude (σ_m, τ_{oct}) of pipe specimen with different thicknesses h have been substituted into Eq. (38) to get the δ. And then, the power law of $\delta \propto h^{-0.20}$ for the epoxy adhesive is obtained in reference to $\delta \propto h^{-0.60}$ for the acrylic adhesive [13] by a least square fitting between log δ and log h. The reference thickness was found when log δ = 0 because the parameters in Eq. (13) are fitted under f = 0. The reference thickness h^* is 0.3 mm for epoxy and 0.4 mm for acrylic. The absolute value of the power exponent of epoxy adhesive is much smaller than that of acrylic adhesive. This result suggests that thickness dependence to the failure of epoxy adhesive is much weaker than that of acrylic adhesive. A new coefficient c_3^* of the failure function which indicates the dependence to the thickness was finally calculated according to Eq. (38) as:

$$c_3^* = b^2\left\{\frac{x_0^2}{a^2} - \left(\frac{h}{h^*}\right)^p\right\}. \quad (39)$$

where p is the power exponent which is -0.20 with $h^* = 0.30$ [mm] for epoxy and -0.60 with $h^* = 0.40$ [mm] for acrylic. By modifying the new coefficient c_3^*, the failure function could be applied to adhesive layer with various thicknesses.

While the thickness dependence is one of the most important structural factors, the material properties of adhered materials are also the other important factor which affects the strength of the adhesive structure. The red curve shown in Fig. 6 (b) is established from the experimental data of multi-material pipes jointed by acrylic adhesive, which consist of SS400 steel pipe and A5052 aluminum pipe with the outer

radius of 45 mm and the thickness of 3 mm. As the numbers of samples are limited, c_1 is set to 0 in the least square fit because the previous result for the single-material pipes [13] gives us the c_1 close to 0. The parameters are finally obtained as $c_1 = 0$ [MPa], $c_2 = 0.0515$ and $c_3 = -19.8$ [MPa^2] under $c_0 = 1.00$ for the multi-material curve and as $c_1 = -0.200$ [MPa], $c_2 = 0.0590$ and $c_3 = -14.0$ [MPa^2] under $c_0 = 1.00$ for the single-material. Comparing the quantities of the parameters, c_1s for both are almost zero and c_2s for both also have similar value with the difference for just 10%. This result shows that the overall shapes of the single-material failure function and the multi-material failure function are almost the same and the only difference is the coefficient c_3. In other words, this difference can be treated as the failure function for adhesive layer with different thickness. As a result, the function can be modified to make them applicable to each other just by changing a new coefficient c_3^* which is modified by h^* according to Eq. (39). If the appropriate h^* is chosen, the multi-material failure curve can be transferred to keep identical with the single-material one which means they have the same property.

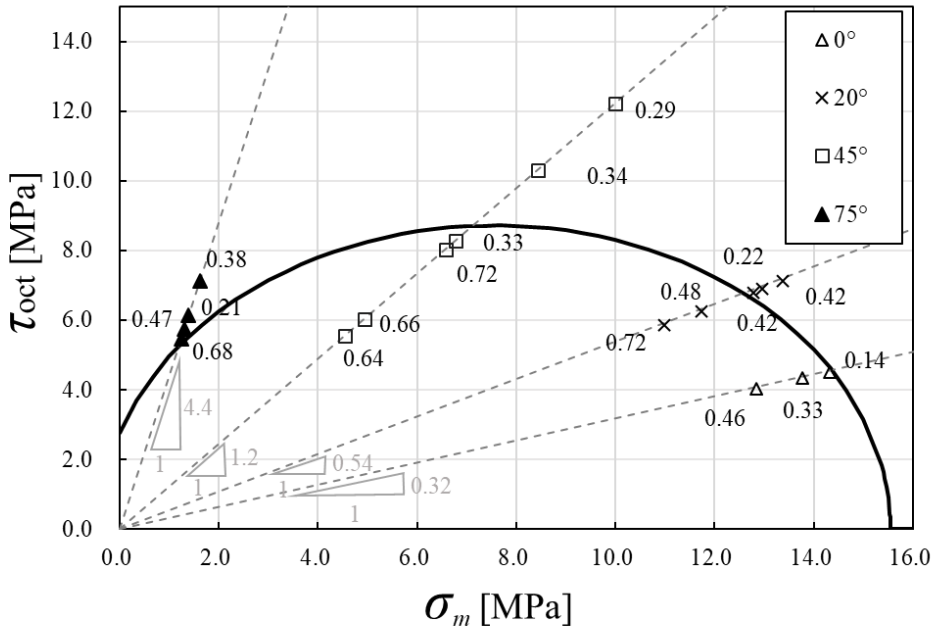

(a) Epoxy adhesive

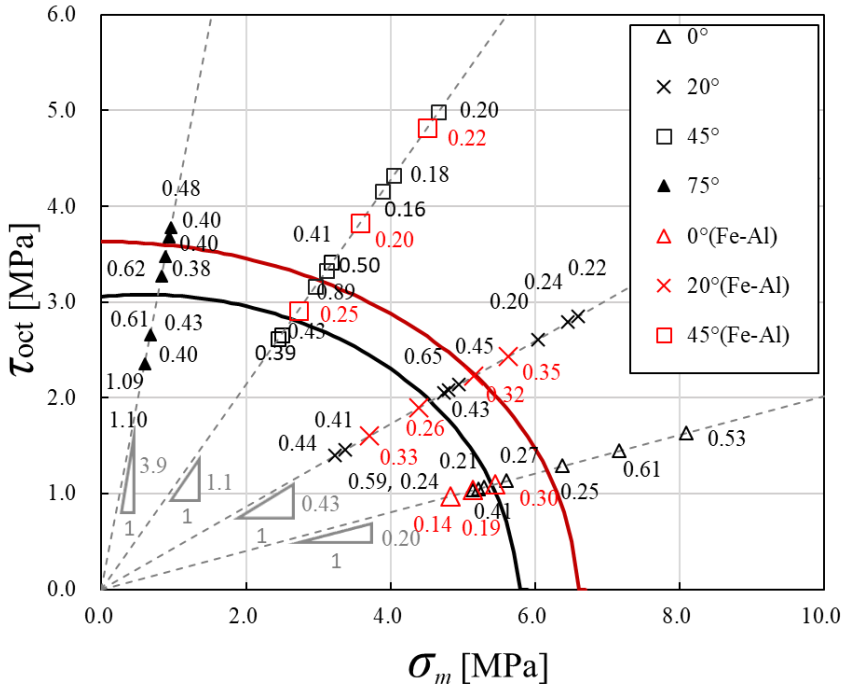

(b) Acrylic adhesive

Figure 6. Failure criterion estimated from experiment results. The number beside the data point shows the average thickness of the adhesive layer of the pipe specimen. (a) Epoxy adhesive (EP-171) (b) Acrylic adhesive (M-600-08), the red data points indicate the experience data collected from pipes with different materials.

Optimal Design of Adhesive Layer

Model and conditions of optimization

A thin-wall pipe joint model which has the thickness of adhesive with 0.13*a*, where *a* is the diameter of pipe (*a* = 20 mm), is used in the optimization calculation as shown in Fig. 7. The elastic properties of adhered materials as well as adhesives are shown in Table 1. In order to simulate the stress state of the bonding between different materials, the upper (A_1 in Fig. 7) and lower (A_2 in Fig. 7) pipes are made of steel and aluminum, respectively. As mentioned in the previous section, there always exists a multiaxial stress state in the adhesive layer so that combined loading conditions should

be considered in optimal design of the adhesive layer. Let α $(= \sigma/\tau)$ be a ratio of tensile stress σ by tension to shear stress τ by torsion, which are applied at both ends of the pipe far from the adhesive region. Three loading conditions are set as shown in Fig. 8. When α = 0, there is only torsion *T*. When α = 2, a combined loading with both torsion *T* and tension *F* applied. When $\alpha \to \infty$, there is only tension *F*.

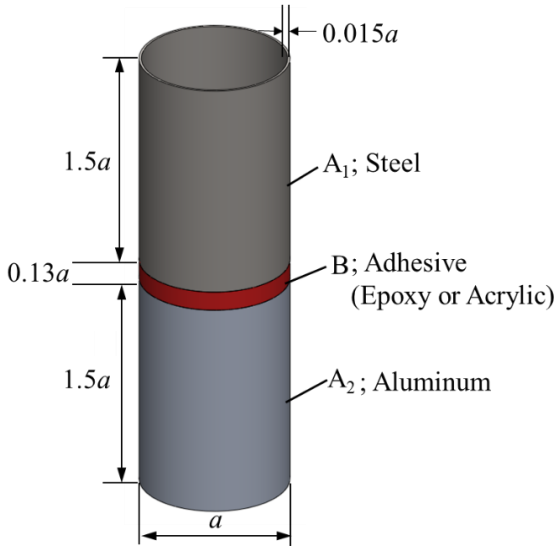

Figure 7. Dimension of the thin-wall pipe model used in the optimization analysis. Two halves are made of different materials and bonded by the adhesives.

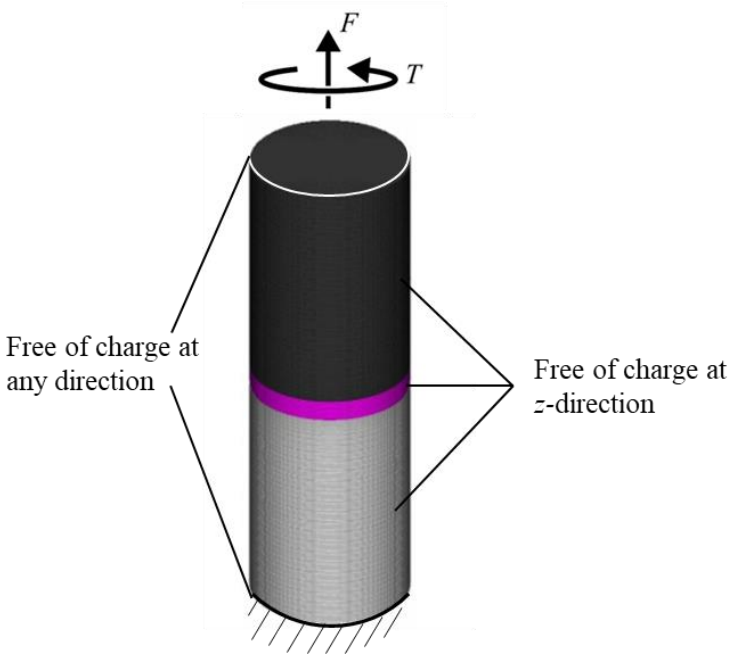

Figure 8. Boundary condition and initial torsion-tension combined load of FEM model.

Material	Young's modulus [GPa]	Poisson's ratio
Steel (A_1)	210	0.3
Aluminum (A_2)	70	0.3
Epoxy adhesive (B)	1.2	0.35
Acrylic adhesive (B)	0.35	0.4

Table 1. Material properties of FEM model

Table 2. Material parameters of failure functions for adhesives (B)

Material	c_0	c_1	c_2	c_3
Epoxy adhesive	1.00	-9.03	0.199	-11.5
Acrylic adhesive	1.00	-0.200	0.0590	-14.0

Comparison on the optimization results

The optimization calculations using epoxy adhesives are obtained under three different loading conditions. These results are compared with the optimization results of acrylic adhesive in ref. [14]. The objective function and volume curves under three loading conditions are shown in Fig. 9. These data are normalized by the initial values of objective function and the volume of the adhesive layer. In most situations, the values of objective functions decrease as the number of iterations increases, which implies the

reasonable success of the minimization. For the cases of epoxy with $\alpha = 0$ and acrylic with $\alpha \to \infty$, the objective functions slightly increase or don't change at all because the original shapes are optimal and thus the initial value of objective function is minimal.

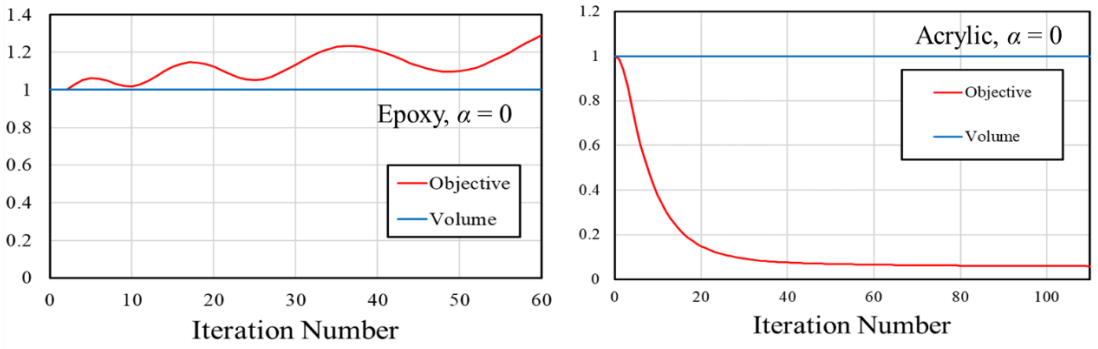

(a) $\alpha = 0$

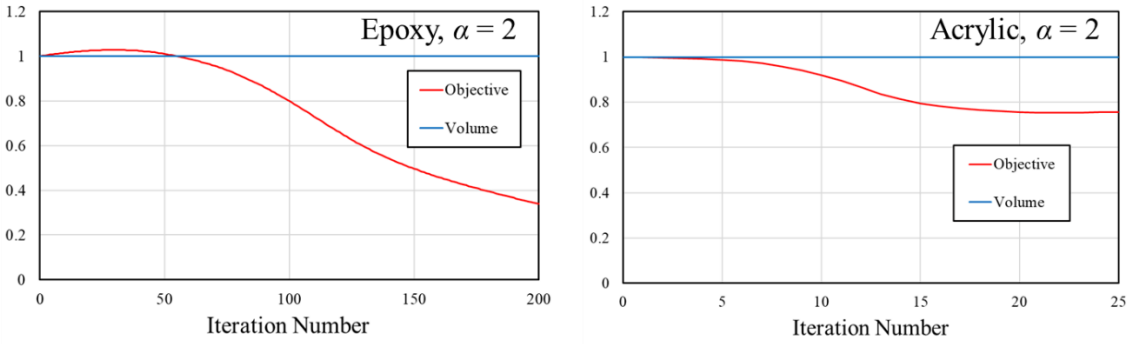

(b) $\alpha = 2$

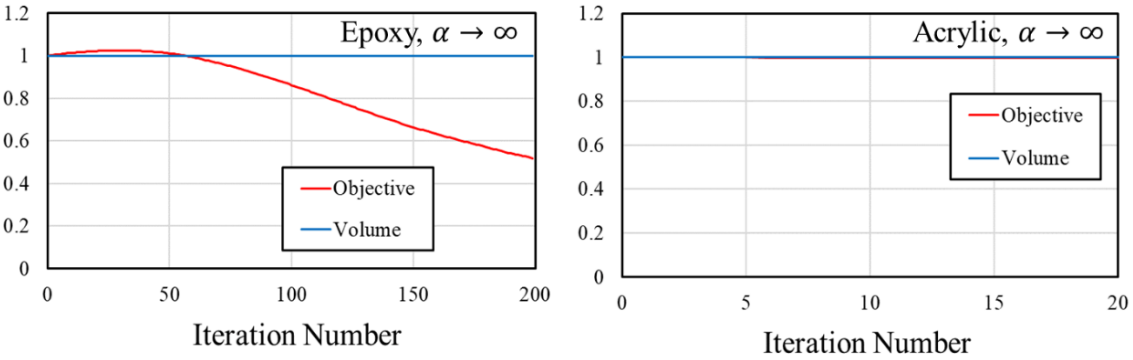

(c) $\alpha \to \infty$

Figure 9. The objective functions according to the iteration number of optimizations under three different loading conditions. (a) $\alpha = 0$, (b) $\alpha = 2$ and (c) $\alpha \to \infty$.

The final shapes of the optimized interfaces of adhesive layers for epoxy and acrylic [14] adhesives are shown in Fig. 10 under the ratios of $\alpha = 0$ (only torsion), 2 and ∞ (only tension). The color map in Fig. 10 gives us equivalent stress (von Mises stress) distribution. From them, the averaged stress of 4.22 [MPa] is rather uniform in most parts of the adhesive layer and this value is much smaller than the averaged stress of 6.67 [MPa] in adhered material A_1 and 6.56 [MPa] in A_2. For different adhesives and different loading conditions, it is found that the optimization of adhesive structure has a strong dependence on the failure function of the employed adhesive material.

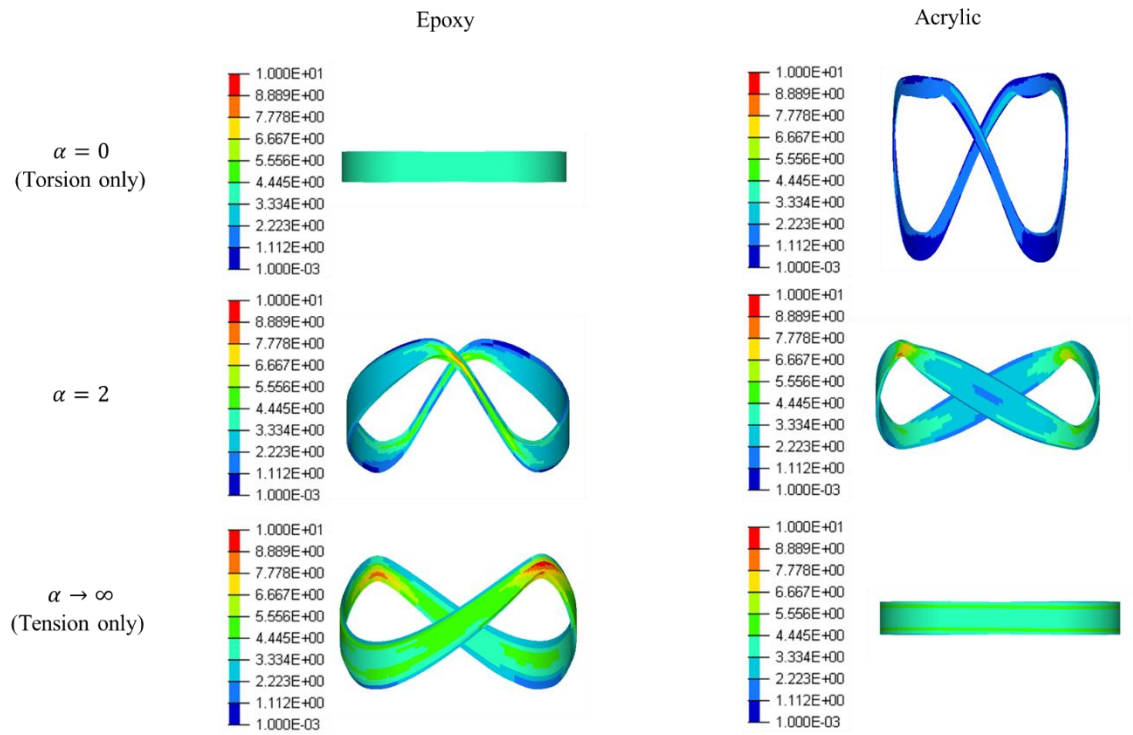

Figure 10. Optimal design of the adhesive layer for epoxy and acrylic adhesives under three different loading conditions.

Optimization process on the failure curve

In order to examine the optimization process in failure space, each step of the optimization is traced. According to Eq. (37), the failure happens when $f = 0$ and

therefore any point $(\sigma_m, \tau_{\mathrm{oct}})$ on the curve indicates the failure state of adhesive. In order to compare the results of optimization with those of experiments, the starting data points of the optimization could be scaled onto the failure curve obtained by experiment data because all the calculations were performed within the linear elasticity. As a result, the initial data points $(\sigma_m^0, \tau_{\mathrm{oct}}^0)$ can be transformed to the modified data points $(\sigma_m, \tau_{\mathrm{oct}})$ on the failure function curve by a multiplier *A* as follows:

$$\frac{\sigma_m}{\sigma_m^0} = \frac{\tau_{\mathrm{oct}}}{\tau_{\mathrm{oct}}^0} = A, \tag{40}$$

where *A* can be calculated by the initial value of $(\sigma_m^0, \tau_{\mathrm{oct}}^0)$ and the parameters of the failure function as follows:

$$A = \frac{-c_1'\sigma_m^0 + \sqrt{(c_1'\sigma_m^0)^2 - 4c_3'\left(c_0'\tau_{\mathrm{oct}}^0 + c_2'{\sigma_m^0}^2\right)}}{2\left(c_0'\tau_{\mathrm{oct}}^0 + c_2'{\sigma_m^0}^2\right)}, \tag{41}$$

On the second issue, optimization is to minimize the objective function in order to increase the strength of the adhesive structure to the failure. The distance of the design data point of the optimization from the origin in the failure space should be shortened so that the data points will get sufficiently inside from the failure curve. According to Fig. 6, the distance to the origin δ in the failure plane of σ_m and τ_{oct} can be calculated as follows because σ_m is orthogonal to τ_{oct} in Haigh–Westergard principal stress space.

$$\delta = \sqrt{\sigma_m^2 + \tau_{\mathrm{oct}}^2}\,. \tag{42}$$

The data points of optimization results were multiplied by *A* and transformed to put the initial point (*n*=0) onto the failure curve. The modified data points through the

optimization processes under three different loading conditions are plotted in the failure space, as shown in Fig. 11. The enlarged views of the optimization processes, (I), (II) and (III), are shown in Fig. 12; (a) region (I) of $\alpha = 0$, (b) region (II) of $\alpha = 2$ and (c) region (III) of $\alpha \to \infty$. The data points for each 10 steps through the optimization iteration were all multiplied by A and the direction of the optimization is shown along arrows. In order to check whether the optimization process minimizes the object function, the distances δ normalized by the initial value of δ_0 are calculated as shown in Fig 13. It is obvious that δ is decreasing as the iteration number n and the process improves the structural integrity of the adhesive layer. The same results for acrylic adhesive in ref. [14] are shown in Fig 14, 15 and 16, respectively. From Figs. 13 and 16, the optimization can reduce the applied stress level for less than 30% from initial shape for the epoxy adhesive and up to 50% for the acrylic adhesive.

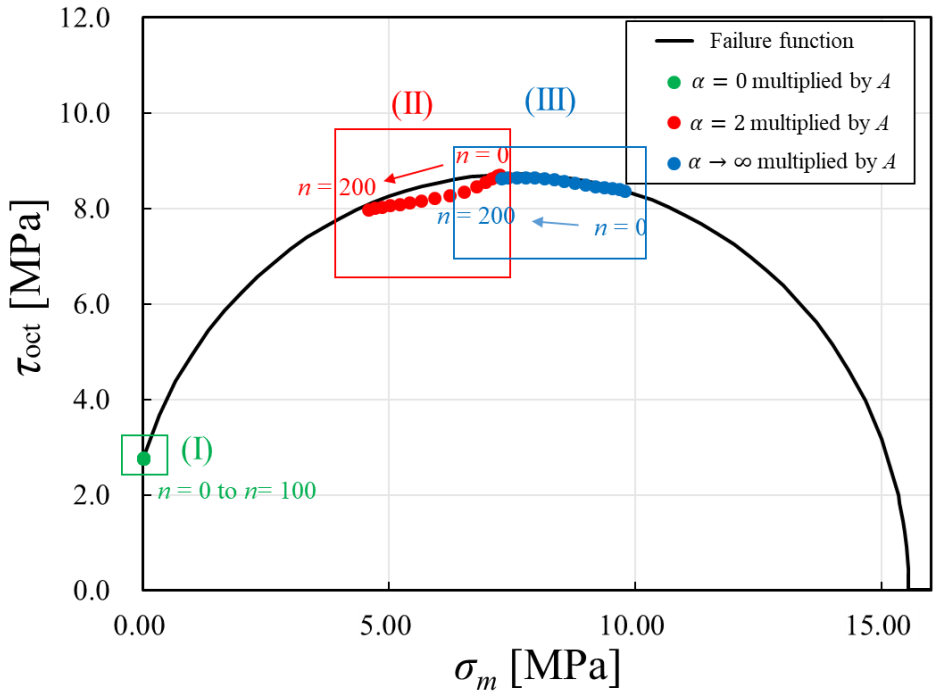

Figure 11. The results of the optimization process on the failure function curve for the epoxy adhesive. The blue dots, red dots and green dots are the results for $\alpha = 0$, $\alpha = 2$ and $\alpha \to \infty$, respectively. n is the iteration number of the optimization.

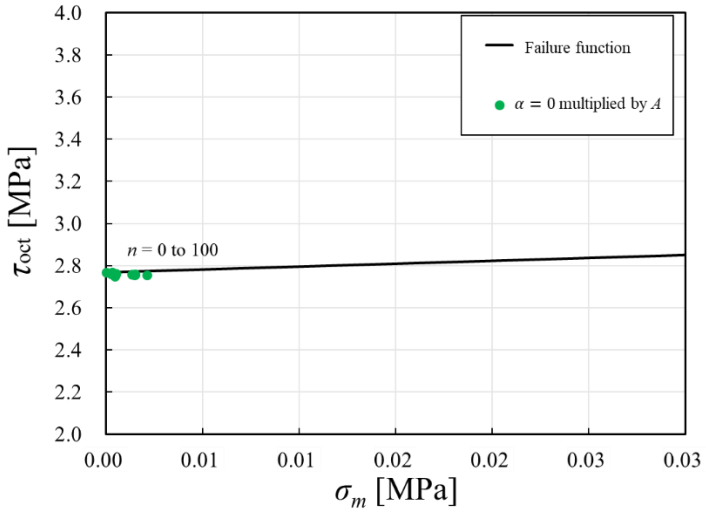

(a) Region (I) in Fig. 11

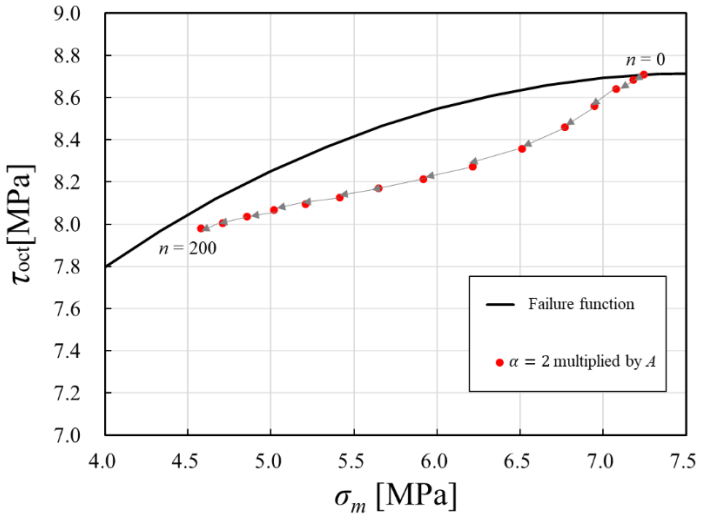

(b) Region (II) in Fig. 11

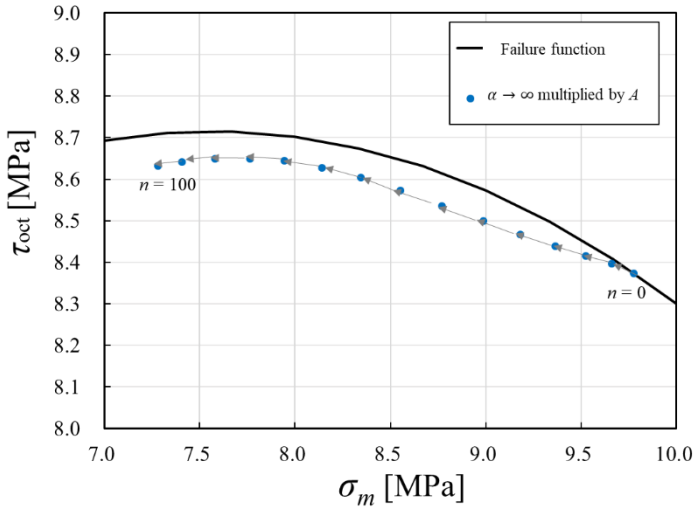

(c) Region (III) in Fig. 11

Figure 12. The enlarged view of the optimization results of the epoxy adhesive multiplied by *A*. (a) Region (I) of $\alpha = 0$, (b) Region (II) of $\alpha = 2$ and (c) Region (III) of $\alpha \to \infty$.

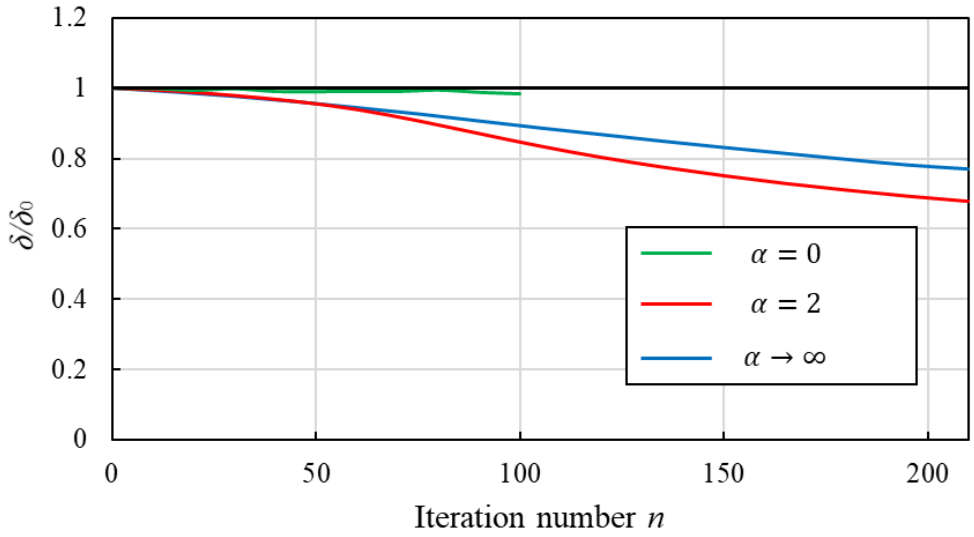

Figure 13. The distance between the data points and the origin for the epoxy adhesive.

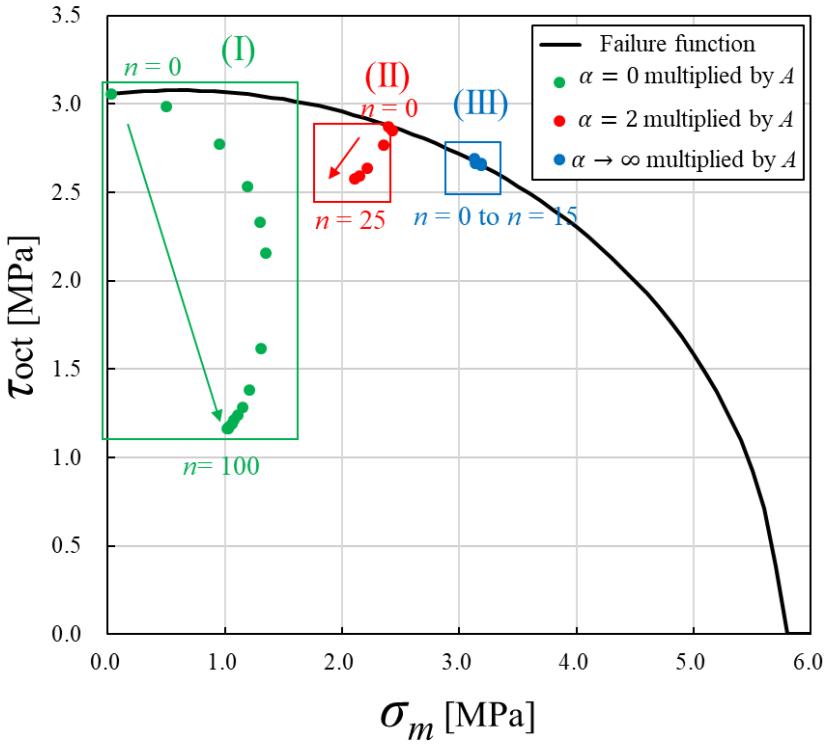

Figure 14. The results of the optimization process on the failure function curve for the acrylic adhesive. The blue dots, red dots and green dots are the results for $\alpha = 0$, $\alpha = 2$ and $\alpha \to \infty$, respectively. n is the iteration number of the optimization.

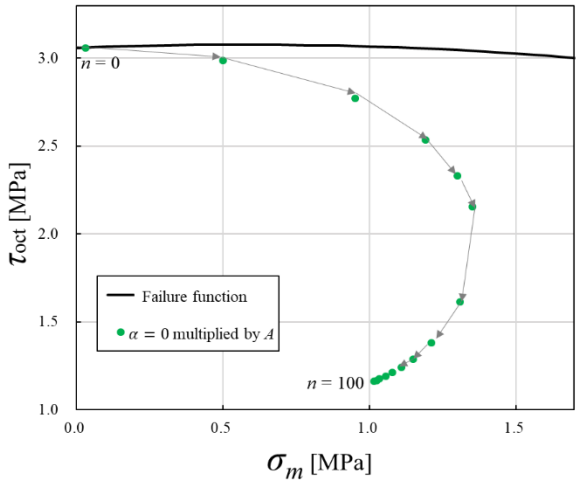

(a) Region (I) in Fig. 14

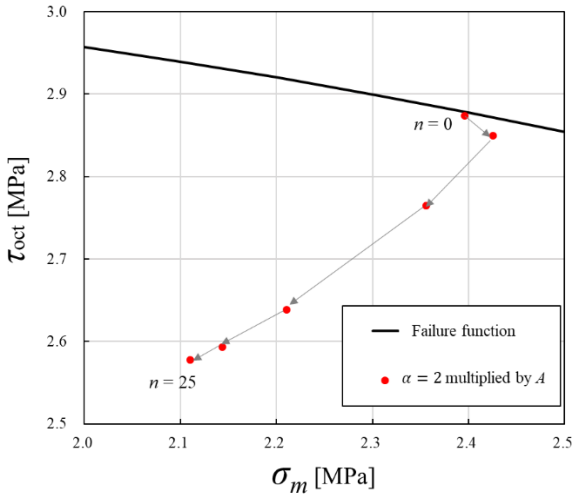

(b) Region (II) 9n Fig. 14

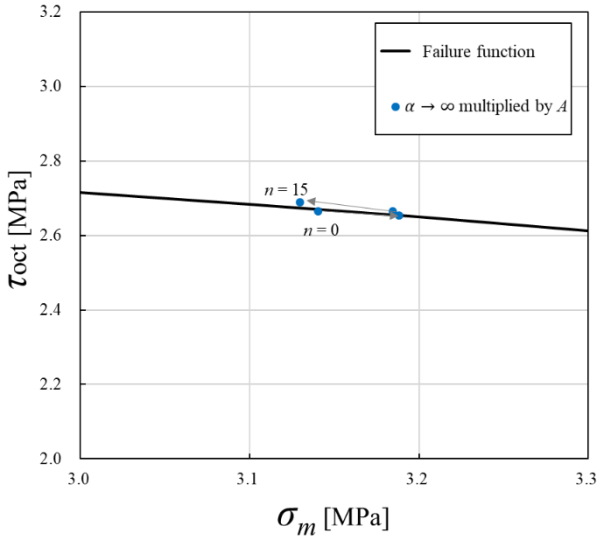

(c) Region (III) in Fig. 14

Figure 15. The enlarged view of the optimization results of the acrylic adhesive multiplied by A. (I) $\alpha = 0$, (II) $\alpha = 2$ and (III) $\alpha \to \infty$.

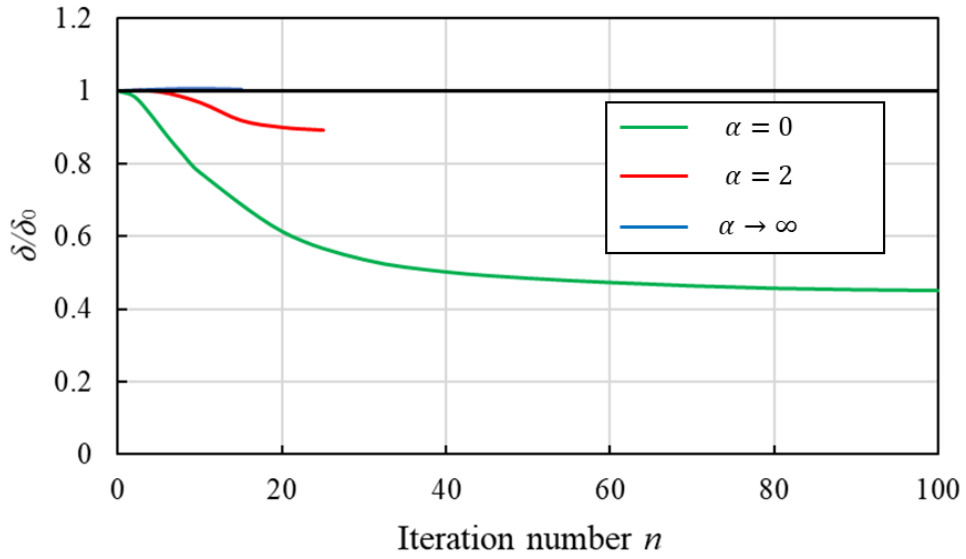

Figure 16. The distance between the data points and the origin for the acrylic adhesive.

Comparing the optimization process of epoxy and acrylic adhesives according to Figs. 12 and 15, the trends of the data points under loading conditions of $\alpha = 0$ and $\alpha \to \infty$ have the most obvious difference. Specifically, for $\alpha = 0$ (only torsion), the data points of epoxy adhesive stay at the original position while those of acrylic adhesive move through the optimization process. For $\alpha \to \infty$ (only tension), the results are totally opposite. The movement of the data points indicates the change of ratio between σ_m and τ_{oct} in the adhesive layer. As the loading applied to the model is kept constant, the ratio of σ_m to τ_{oct} observed in the adhesive layer can only be changed by the shape change of the adhesive layer. Looking back in Fig. 10, the shape of layer for the epoxy adhesive stays the original shape under $\alpha = 0$ and the shape of that for the acrylic adhesive keeps the original shape under $\alpha \to \infty$. Considering the reason for these optimized behaviors, the shape gradient function of Eq. (30), has been investigated. According to Eq. (30), l_G, which is calculated by the shape gradient function, indicates the change rate of the work done by the driving force on the adhesive interface which causes the shape change of the adhesive layer. The values of l_G through the first several steps of the optimization

process for epoxy and acrylic adhesives are obtained, as shown in Fig. 17 for $\alpha = 0$ and Fig. 18 for $\alpha \to \infty$, respectively. The red line shows the result of epoxy adhesive and the blue line shows that of acrylic adhesive. For $\alpha = 0$, the value of shape gradient function for acrylic adhesive is positive so that the driving force causes the shape change along the positive direction and then the angle of the adhesive layer gets larger. However, for epoxy adhesive, the value of shape gradient function is negative so that this optimization is impossible. As a result, the shape of the adhesive layer only stays at the initial one. For $\alpha \to \infty$, the value of shape gradient function is positive for epoxy adhesive but negative for acrylic adhesive so that the shape change has an opposite pattern with that of $\alpha = 0$. This fact concludes that the initial shape for optimization is strongly affected to the final shape and the shape gradient function is the definite indicator wherever the present initial model is appropriate or not for the multi-material design.

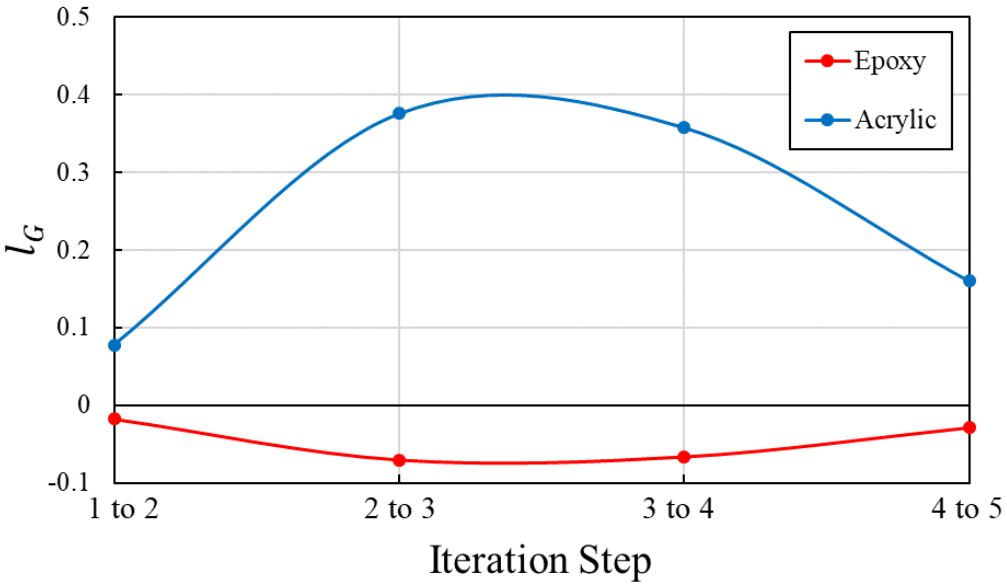

Figure 17. The shape gradient function of epoxy and acrylic adhesives for the first 5 steps of optimization under the loading condition $\alpha = 0$.

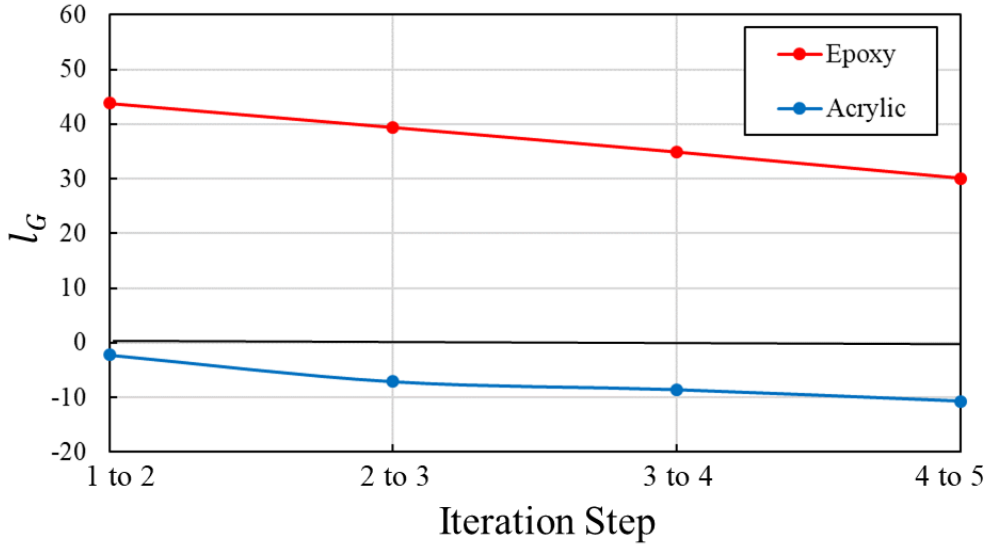

Figure 18. The shape gradient function of epoxy and acrylic adhesives for the first 5 steps of optimization under the loading condition $\alpha \to \infty$.

Conclusions

The failure criterion expressed by the first invariant of stress tensor I_1 and the second invariant of deviatoric stress tensor J_2 for epoxy adhesive was obtained from experimental data using a simple uniaxial tensile test and plotted into the failure plane of σ_m from I_1 and τ_{oct} from J_2. The result was compared with the case for acrylic adhesive in reference [13]. The failure function of the epoxy adhesive has the center of ellipse failure curve with $\sigma_m = 22.7$ [MPa] while the acrylic does not have such a point. The major axis in the σ_m direction is almost 3 times and the axis in the τ_{oct} direction perpendicular to the former axis is 2.5 times larger than those of the acrylic adhesive. Therefore, both adhesives have the strong difference of the failure properties.

Shape optimization problem that would improve the strength of the adhesive structure in multiaxial stress state, was proposed reflecting the difference between both failure functions of adhesive materials. The distances of the design data point from the origin in the failure plane of σ_m and τ_{oct} decrease through the optimization for both

adhesives, indicating that the optimization process satisfies the minimization of objective function. The optimal shape can reduce the applied stress level for less than around 30% from the initial one for the epoxy adhesive and 50% for acrylic. We found that these final shapes are numerically optimized to realize the higher mechanical integrity of the adhesive layer. The shape gradient function which induces the geometric change of the adhesive layer is the driving force under the applied mean stress and shear stress. The shapes of the adhesive layers have been not changed for epoxy adhesive under $\alpha = 0$ and acrylic adhesive under $\alpha \to \infty$ because of the negative value of the shape gradient function and it becomes the indicator where the initial model is appropriate or not for the multi-material design.

Acknowledgements

This research also got the help from Yoshiki Yamauchi (Sumitomo Chemical Co., Ltd.) who graduated from Osaka University in March 2021. We also thanks Akoo Mechanical Engineering Co., Ltd. for providing the pipe specimens.

Reference

[1] Goede, M., Stehlin, M., Rafflenbeul, L., Kopp, G. and Beeh, E., *European Transport Research Review*, **1**, No. 1, 5-10 (2009).

[2] Katayama, S. and Kawahito, Y., *Scripta. Mater.* **59**, 1247–1250 (2008).

[3] Liyanage, T., Kilbourne, J., Gerlich, A. P., and North, T. H., *Sci. Technol. Welding Joining*, **14**, 500–508 (2009).

[4] Kawasaki, S., Nakajima, G., Haraga, K., and Sato, C., *J. Adhes.*, **92**, 517–534 (2016).

[5] Colin H, S. Dennis E, M. and Neil, P., *Manual of Engineering Drawing (Fifth Edition),* 547-560 (2020).

[6] Kinloch, A., *J. Adhesion and Adhesives: Science and Technology. London: Chapman and Hall, Ltd,* p. 26, 139, 365 (1987).

[7] Yohannes L. Yaphary, Zechuan Y., Raymond H.W. L., David H. and Denvid L., *Composites Part B: Engineering,* **131**, 165-172 (2017).

[8] Brewer, J. C. and Lagace, P. A., *J. Compos. Mater.* **22**, 1141–1155 (1988).

[9] Mahnken, R. and Schlimmer, M., Int. *J. Numer. Methods Eng.* **63**, 1461–1477 (2005).

[10] Richardson, D. E., McLennan, M. L., Anderson, G. L., Macon, D. J., and Batista-Rodriguez, A., *J. Adhes.* **79**, 157–174 (2003).

[11] Dolev, G. and Ishai, O., *J. Adhes.* **12**, 283–294 (1981).

[12] Adams, R. D., Atkins, R. W., Harris, and J. A., Kinloch, A. J., *J. Adhes.* **20**, 29–53 (1986).

[13] M. Iimori, H. Tanaka, M. Kimura, Y. Shibutani, and Y. Liu, *Mechanical Eng. J.*, **5**, 17-00577 (2018).

[14] M. Iimori, H. Tanaka, Y. Shibutani, and Y. Liu, *Trans. JSME (in Japanese)*, **85**, 18-00409 (2019).

[15] Pinto, A. M. G., Magalhães, A. G., Campilho, R. D. S. G., De Moura, M. F. S. F., and Baptista, A. P. M., *J. Adhes.* **85**, 351–376 (2009).

[16] Adams, R. D., *J. Adhes.* **30**, 219–242 (1989).

[17] Ikegami, K. and Sugibayashi, T., *J. Adhes.* **21**, 211–227 (1987).

[18] Kaelble, D. H., *J. Adhes.* **37**, 205–214 (1992).

[19] Thouless, M. D. and Jensen, H. M., *J. Adhes.* **38**, 185–197 (1992).

[20] Chai, H., *Int. J. Fract.* **60**, 311–326 (1993).

[21] Chai, H., *Int. J. Fract.* **130**, 497–515 (2004).

[22] Bossler, F. C., Franzblau, M. C., and Rutherford, J. L., *J. Sci. Instrum. (J. Phys. E)*, **1**, 829–833 (1968).

[23] Liechti, K. M. and Hayashi, T., *J. Adhes.* **29**, 167–191 (1989).

[24] Teutenberg, D., Meschut, G., Schlimmer, M., Kroll, U., and Matzenmiller, A., *Annu. Meeting Program Adhes. Soc.* (2013).

[25] Spaggiari, A., Castagnetti, D., and Dragoni, E., *J. Adhes.* **89**, 660–675 (2013).

[26] R. J. Green, *Int. J. Mech. Sci.*, **14**, 215–224 (1972).

[27] J. C. Brewer and P. A. Lagace, *J. Comp. Mat.*, **22**, 1141–1155 (1988).

[28] Azegami, H., *Trans. JSME* (in Japanese), **60**, 1479-1486 (1994).

[29] da Silva, Lucas F. M., Rodrigues, T. N. S. S., Figueiredo, M. A. V., de Moura, M. F. S. F., and Chousal, J. A. G., *J. Adhes.* **82**, 1091–1115 (2006).

[30] Tanaka, H., Kimura, M., Iimori, M., Shibutani, Y., and Liu, Y., *Key Eng. Mater*. 725, 383–388 (2017).